Letter

Femtosecond dynamics of electrons in noble metals: Orientational relaxation in momentum space and the Drude relaxation rate

Jonas Grumm [*] and Andreas Knorr [†]

Nichtlineare Optik und Quantenelektronik, Institut für Physik und Astronomie, Technische Universität Berlin, 10623 Berlin, Germany

(Received 29 April 2025; revised 1 October 2025; accepted 3 November 2025; published 1 December 2025)

We investigate the momentum-resolved dynamics of conduction electrons in noble metals following ultrashort optical excitation with linearly polarized light. Using a momentum-resolved Boltzmann equation approach for electron-phonon interaction, we solve for the combined effects of orientational relaxation, thermalization, and cooling. We introduce momentum orientational relaxation as the initial step in the equilibration of an optically excited nonequilibrium electron gas by highlighting its importance for the optical response of noble metals as the dephasing of the Drude model. The numerical results for gold reveal that orientational relaxation exists already for linear optical excitations and dominates on time scales on the first tens of femtoseconds after excitation. Also incorporating thermalization and cooling on times up to a few picoseconds, our approach provides a simultaneous description of optical and thermal properties of noble metals under optically induced nonequilibrium conditions.

DOI: 10.1103/nq66-bzwj

Introduction. In recent years, the development of ultrashort laser pulses made it possible to observe the dynamical optical response of solids with femtosecond resolution and provided insights into the build up and decay of nonequilibrium electronic or plasmonic excitations in noble metals [1–6]. The relaxation back to a thermodynamic equilibrium, which proceeds in noble metals on scales from a few fs to several ps, depends strongly on the excitation conditions. The relaxation of the nonequilibrium energy-resolved electron distribution itself can be divided in thermalization by electron-electron and electron-phonon interaction [7], dissipation (electron cooling) by electron-phonon interaction [8–13], and lattice cooling by phonon-phonon interaction [14,15]. These processes are addressed in many publications by effective macroscopic models [16–20] or microscopic theories based on the semiclassical Boltzmann equation where the electron states are numbered by energy [7–13,21–24].

These energy-resolved approaches neglect the fact that the polarization of the exciting light field breaks the symmetry of the momentum distribution of the initially isotropic electron gas. This symmetry break corresponds to an anisotropic excitation of electronic momentum which cannot be addressed in an energy-resolved basis only. However, the recent development of pulses as short as several fs should make it possible to perform momentum-resolved measurements by orthogonal polarized pump-probe spectroscopy [25] or time-resolved ARPES [26].

[*]Contact author: j.grumm@tu-berlin.de

[†]Contact author: andreas.knorr@tu-berlin.de

In this Letter, we introduce the orientational relaxation of the momentum-polarized conduction electrons in noble metals as first equilibrization step after optical excitation with linearly polarized light (cf. Fig. 1). We show that orientational relaxation is fundamental for the optical response of noble metals [27], acts as dephasing of collectively excited electrons, effects the relaxation dynamics up to 100 fs after the excitation, and represents an important parameter in the Drude model. So far, to our knowledge, momentum orientational relaxation has not been discussed much beyond the relaxation time approximation [28–32] but occurs on the same footing with thermalization and cooling of a nonequilibrium electron gas as a first dephasing process. To tackle this problem, we consider the numerical solution of a momentum-resolved Boltzmann equation exemplarily for gold including light-matter interaction and electron-phonon scattering [27]. This approach includes orientational relaxation, thermalization as redistribution of electronic energy and cooling as energy dissipation from electrons to phonons. To study a well defined situation, all three processes are described by a consistent treatment of the electron-phonon interaction via normal and umklapp processes. In the following, we will discuss these three relaxation processes in terms of the dynamics of the electron distribution, introduce characteristic time scales via observables and connect orientational relaxation with the well-known Drude model.

Theory. For the description of the dynamics of electrons in the sp-conduction band of noble metals after optical excitation, we apply a parabolic and isotropic dispersion $\epsilon_k = \frac{1}{2m}\hbar^2|\mathbf{k}|^2$ at their Fermi edge with an effective mass m initially at room temperature $T_{\mathrm{eq}} = 300$ K. For optical excitations below the electronic band gap, this description via intraband excitations is sufficient [31–33]. Dissipative processes are incorporated via electron-phonon interaction [8,11,34,35]. By introducing the microscopic electronic conduction band occupations $f_{\mathbf{k}}$ with momentum $\mathbf{k}$, we obtain

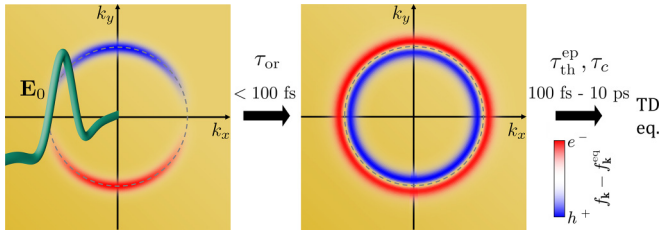

FIG. 1. Schematics of the electron relaxation processes: Left: A linear polarized light field $\mathbf{E}_0$ induces a momentum-polarization of the electron distribution $f_{\mathbf{k}}$ creating excited intraband electrons and holes near the Fermi edge (dashed circle). The excited nonsymmetric distribution decays in the orientational relaxation time τ_{or} into a symmetric distribution. Right: The relaxation back into the thermodynamic equilibrium (TD Eq.) proceeds in the thermalization and cooling time ($\tau_{\mathrm{th}}^{\mathrm{ep}}$, τ_c). The thickness of the colored areas is magnified by a factor of 20 in comparison to the radius of the Fermi sphere for better visibility.

[27] the momentum-resolved Boltzmann equation [13,15,36]

$$\partial_t f_{\mathbf{k}} = \frac{e}{\hbar}\mathbf{E}_0(t)\cdot\nabla_{\mathbf{k}} f_{\mathbf{k}} + \Gamma_{\mathbf{k}}^{\mathrm{in}}(1-f_{\mathbf{k}}) - \Gamma_{\mathbf{k}}^{\mathrm{out}} f_{\mathbf{k}}, \tag{1}$$

where the electron-phonon scattering rates are $\Gamma_{\mathbf{k}}^{\mathrm{in}} = \sum_{\mathbf{k}'} W_{\mathbf{k}'\to\mathbf{k}} f_{\mathbf{k}'}$, $\Gamma_{\mathbf{k}}^{\mathrm{out}} = \sum_{\mathbf{k}'} W_{\mathbf{k}\to\mathbf{k}'}(1-f_{\mathbf{k}'})$ and

$$W_{\mathbf{k}\to\mathbf{k}'} = \frac{2\pi}{\hbar}\sum_{\mathbf{G},\pm}\left|g_{\mathbf{k}-\mathbf{k}'}^{\mathbf{G}}\right|^2 \delta(\epsilon_{\mathbf{k}'} - \epsilon_{\mathbf{k}} \pm \hbar\omega_{\mathbf{k}-\mathbf{k}'+\mathbf{G}}) \times \left(\frac{1}{2} \pm \frac{1}{2} + n(\hbar\omega_{\mathbf{k}-\mathbf{k}'+\mathbf{G}})\right) \tag{2}$$

as scattering amplitude. Equation (1) is nonlinear in the electron occupations $f_{\mathbf{k}}$ due to Pauli blocking $(1-f_{\mathbf{k}'})$ as derived in Ref. [27]. The phonon density $n(\hbar\omega_{\mathbf{k}-\mathbf{k}'+\mathbf{G}})$ (phonon energy $\hbar\omega_{\mathbf{k}-\mathbf{k}'+\mathbf{G}}$) is treated here as a thermal bath within a Bose-Einstein distribution. This is justified by analyzing a two-temperature model [37–40] with similar initial conditions after the impulsive excitation as in the results discussed below. However, in principle the phonon dynamics can be addressed in the same way as the electron dynamics [9,10]. Incorporating normal and umklapp processes via reciprocal lattice vectors $\mathbf{G} \neq 0$, we apply a screened electron-phonon coupling $g_{\mathbf{k}-\mathbf{k}'}^{\mathbf{G}}$ [27].

The excitation by the incident light field $\mathbf{E}_0$ is described here as a function of the polarization direction and not via the direction-independent intensity as in previous approaches focusing on energy relaxation out of a momentum-isotropic situation [7–13,21–24]. The latter is encoded in the intraband dipole coupling $\mathbf{E}_0\cdot(ie\nabla_{\mathbf{k}})$ for Bloch electrons [27,41]: The light field breaks the symmetry of the momentum distribution by the distinct polarization direction of $\mathbf{E}_0$. Disturbing the initial isotropy of the momentum distribution selectively, this opens the possibility to study orientational relaxation as a new relaxation/dephasing channel.

The Boltzmann equation (1) is solved numerically with methods presented in Appendix F in Ref. [27] and gold parameters listed in Table 1 in Ref. [27]. In the following, we investigate the combined dynamics of electron relaxation in terms of orientational relaxation, thermalization, and cooling after optical excitation in a bulk system (cf. Fig. 1). To illustrate this sequence of relaxation processes, we apply a linearly y-polarized light field $\mathbf{E}_0$ represented by a single Gaussian pulse with a duration of 12 fs (FWHM) and a carrier frequency of 5 THz so that only a half oscillation cycle contributes to excitation. On the expected time scale of the relaxation dynamics described above, the chosen pulse acts only as an initial condition which allows to study the sequence of the intrinsic electron relaxation without the influence of an ongoing fast shaking of the distribution on the oscillation frequency.

In the following, we will study linear and nonlinear excitation regimes. Both regimes can be distinguished via the distortion of the electron distribution, i.e., by the acceleration energy ϵ_{ac} the electrons gained from the incident light field (cf. Ref. [27]) in comparison with the thermal broadening of the Fermi edge $k_B T_{\mathrm{eq}}$: In the regime of nonlinear excitations, the field strength is set to $E_0 = 0.7\ \frac{\mathrm{MV}}{\mathrm{cm}}$ ($\epsilon_{\mathrm{ac}} \gtrsim k_B T_{\mathrm{eq}}$), while for linear excitations $E_0/100$ ($\epsilon_{\mathrm{ac}} \ll k_B T_{\mathrm{eq}}$) is assumed. In this context, we expect that orientational relaxation without any energy exchange with the phonon system exists across all excitation regimes, while thermalization and cooling as energy relaxation processes occur only in the nonlinear regime.

Qualitative discussion. The light-matter interaction in the Boltzmann equation (1) breaks the original radial symmetry of the electron distribution in momentum space, since electrons are initially accelerated in the polarization direction $\mathbf{e}_y$ of the half cycle pulse $\mathbf{E}_0$. Counteracting to this, the electron-phonon interaction does not prefer any direction and thus starts to equilibrate all momentum orientations to a distribution of uniform momentum directions. To analyze this process, we divide the electron distribution into a nonsymmetric distribution $f_{k_x,k_y,k_z}^{\text{non-sym}}$ depending on the direction of the momentum $\mathbf{k} = (k_x, k_y, k_z)^T$ and a symmetric distribution $f_{|\mathbf{k}|}^{\mathrm{sym}}(t)$ depending on the momentum absolute $|\mathbf{k}|$:

$$f_{\mathbf{k}}(t) = f_{k_x,k_y,k_z}^{\text{non-sym}}(t) + f_{|\mathbf{k}|}^{\mathrm{sym}}(t), \tag{3}$$

$$f_{|\mathbf{k}|}^{\mathrm{sym}}(t) = f_{|\mathbf{k}|}^{\text{non-th}}(t) + f_{|\mathbf{k}|}^{\mathrm{th}}(t). \tag{4}$$

Later in Eq. (4), to distinguish thermalization and cooling, the symmetric distribution $f_{|\mathbf{k}|}^{\mathrm{sym}}$ is divided into thermal $f_{|\mathbf{k}|}^{\mathrm{th}}$ and nonthermal $f_{|\mathbf{k}|}^{\text{non-th}}$ components [22,42].

Thus, as illustrated in Fig. 1, orientational relaxation applies to the fact that the nonsymmetric electron distribution $f_{k_x,k_y,k_z}^{\text{non-sym}}$ induced by the light field $\mathbf{E}_0$ is driven into a symmetric distribution $f_{|\mathbf{k}|}^{\mathrm{sym}}$, which does not prefer a direction in momentum space. Our numerical results indicate that this process of momentum orientational relaxation occurs already for vanishing acceleration energy ϵ_{ac} in the linear regime and remains important for nonlinear excitation. To illustrate this process, Figs. 2(a) and 2(b) depict the temporal occupation dynamics in the k_x and k_y directions (orthogonal and parallel to the incident light polarization) for three different momentum states located close to the Fermi edge (k_x and k_z directions show the same dynamics). To enhance the visibility of this process, we depict in Fig. 2 only the results for the nonlinear excitation with strength E_0 where the electron gas is strongly perturbed. Nevertheless, in the linear regime, orientational relaxation shows the same qualitative signatures.

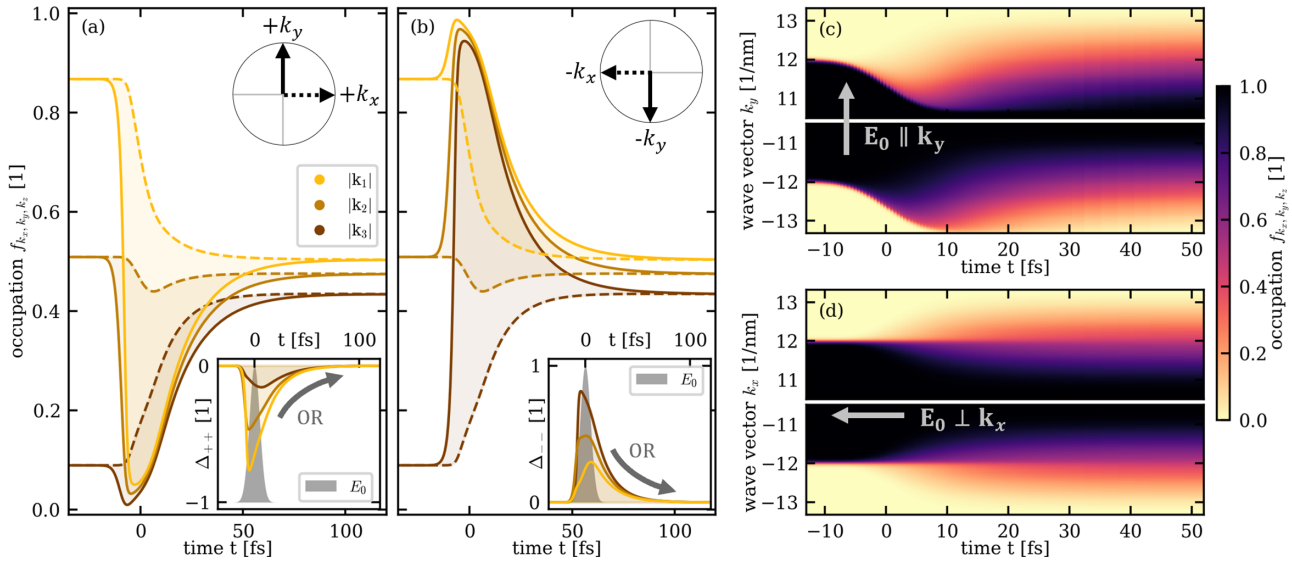

FIG. 2. Momentum-resolved electron dynamics after excitation within positive y-direction polarized field with strength E_0. In (a), (b) the occupation of three k_x (dashed lines) and k_y (solid lines) momentum states located in the region of thermal broadening close to the Fermi edge at $|\mathbf{k}_1| = k_F - 0.05\ \mathrm{nm}^{-1}$, $|\mathbf{k}_2| = k_F = 12.0\ \mathrm{nm}^{-1}$, and $|\mathbf{k}_3| = k_F + 0.05\ \mathrm{nm}^{-1}$ are shown. In (a), a depopulation of states in positive k_y direction (with $k_x = k_z = 0$) occur, whereas the dynamics in positive k_x direction (with $k_y = k_z = 0$) is delayed due to electron-phonon scattering. In contrast, (b) shows for the negative k_y direction (with $k_x = k_z = 0$) an overpopulation, but the same behavior for the negative k_x direction (with $k_y = k_z = 0$) as in (a). The insets in (a), (b) reveal orientational relaxation (OR) as decay of the occupation difference $\Delta_{\pm\pm} = f_{0,\pm k_y,0} - f_{\pm k_x,0,0}$, whereby all three states show similar relaxation behavior. The gray shaded areas show the excitation pulse E_0. The electron distribution in momentum space is depicted along the (c) k_y and (d) k_x axis (the k_z direction is identical with the k_x case) and represents a Fermi-Dirac distribution in equilibrium.

Out of the initial equilibrium Fermi-Dirac distribution $f_k^{\mathrm{eq}}(T_{\mathrm{eq}})$ during the first tens of fs after the excitation, the occupations in Figs. 2(a) and 2(b) clearly show a nonsymmetric behavior of the distribution $f_{\mathbf{k}}$ with respect to k_x (dashed) and k_y directions (solid). Thereby, due to the accelerating Lorentz force, Eq. (1), and the distinct polarization direction $\mathbf{E}_0 \parallel \mathbf{e}_y$, states in the positive k_y direction reveal an electron depopulation, whereas in the negative k_y direction, conversely, an overpopulation emerges (cf. also left of Fig. 1). The onset of the dynamics in the k_x direction is temporally delayed compared to the k_y direction which is initially displaced by the light field on the scale of the pulse duration of 12 fs. After the orientational relaxation time τ_{or} of less than 100 fs the directional dependence of f_{k_x,k_y,k_z} is synchronized [cf. insets in Figs. 2(a) and 2(b)], i.e., equilibrated with respect to the momentum direction, and has developed into a symmetric distribution depending only on $|\mathbf{k}|$, i.e., on energy ϵ_k. Such an orientational relaxation has already been studied in the semimetal graphene [43,44], photoexcited semiconductors [45] or on the basis of a relaxation time approximation in metals [30,31], but as far as we know, has not been discussed much quantitatively for noble metals in terms of the full nonlinear electron dynamics such as Eq. (1). In Figs. 2(c) an 2(d), the evolution of the full electron distribution $f_{\mathbf{k}}$ as a function of k_y and k_x is visualized in time and momentum space. Initially, before excitation at $t = 0$, Figs. 2(c) and 2(d) show a Fermi-Dirac distribution in equilibrium with the phonon bath and a Fermi level at $k_F = 12.0\ \mathrm{nm}^{-1}$ (dark areas describe occupied electron states and bright areas unoccupied states). On the time scale of the excitation pulse in Fig. 2(c), the strong displacement of the electron distribution parallel to the polarization of the light field in the k_y direction is visible.

The strong de- and overpopulation of the states in the k_y direction [cf. Figs. 2(a) and 2(b)], however, only occur in the nonlinear regime, where the equilibrium Fermi-Dirac distribution is disturbed significantly at the Fermi edge.

In this way, the nonlinear excitation regime opens the possibility to test the momentum polarization and orientational relaxation with experimental techniques such as orthogonal polarized pump-probe spectroscopy [25] or time-resolved ARPES [26].

While in the linear regime the electron gas reaches thermodynamic equilibrium after orientational relaxation, in the nonlinear regime energy relaxation continues: Energy relaxation includes thermalization as redistribution of the nonthermal electronic energy into a thermal one and cooling as energy dissipation to the phonon bath [11,22]. The processes of thermalization and cooling as a function of energy are well studied in literature [8–11,22,23]. Here, we only show that they develop in a consistent fashion out of the same theory as the orientational relaxation, i.e., by solving Eq. (1) in a momentum-resolved picture.

After the orientational relaxation, the nonsymmetric distribution $f_{k_x,k_y,k_z}^{\text{non-sym}}$ is decayed completely and electrons are distributed symmetrically $f_{|\mathbf{k}|}^{\text{sym}}$ but not necessarily thermal (i.e., non-Fermi-Dirac), cf. Eq. (4), and an energy-dependent representation of the distribution in terms of $\epsilon_k = \frac{1}{2m}\hbar^2|\mathbf{k}|^2$ is permissible. In the next step, the transition from a nonthermal distribution $f_{|\mathbf{k}|}^{\text{non-th}}$ into a thermal Fermi-Dirac distribution $f_{|\mathbf{k}|}^{\text{th}}$ due to electron-phonon scattering proceeds in the

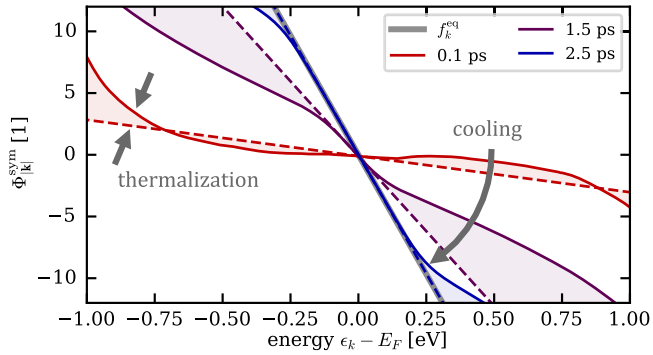

FIG. 3. The quasilogarithmic representation of the symmetric distribution $\Phi^{\rm sym}_{|\mathbf{k}|}$ (solid lines) reveals the thermal (dashed lines) and nonthermal distribution (shaded areas). The nonthermal distribution at 0.1 fs is scaled by a factor of four for better visualization. At 2.5 ps the thermal distribution superimposes with the equilibrium distribution $f_k^{\rm eq}$ (gray line).

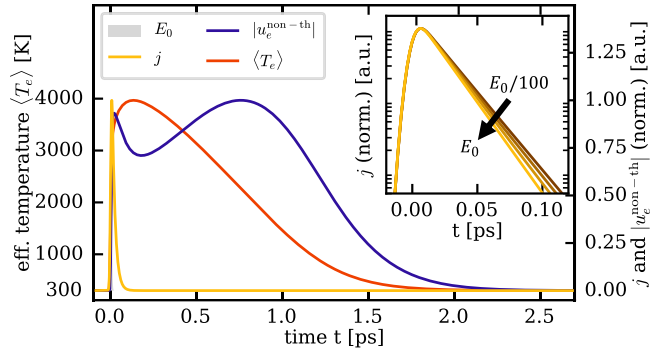

FIG. 4. The current density j decays exponentially within the orientational relaxation time $\tau_{\rm or}$. On longer time scales, the nonthermal energy density $|u^{\rm non\text{-}th}|$ and effective temperature $\langle T_e \rangle$ track thermalization and cooling. The inset shows the decay of the current density for different excitation strengths from $E_0/100$ (dark) to E_0 (bright).

thermalization time $\tau_{\rm th}^{\rm ep}$. At the same time, the excited hot electron gas dissipates its thermal energy to the phonon system in the cooling time τ_c.

To distinguish between the simultaneously proceeding thermalization and cooling processes, we introduce the quasilogarithmic representation $\Phi^{\rm sym}_{|\mathbf{k}|} = -\ln\left((f^{\rm sym}_{|\mathbf{k}|})^{-1} - 1\right)$ of the symmetric distribution as in Ref. [10]. This function connects a thermal Fermi-Dirac distribution linearly to the electron energy ϵ_k with slope proportional to the inverse electron temperature T_e^{-1}. The solid lines in Fig. 3(a) illustrate our numerical result for different times after excitation with the corresponding thermal distribution $f^{\rm th}_{|\mathbf{k}|}$ as fitted Fermi-Dirac distribution (dashed lines). Their increasing slope over time consequently describes the cooling of the electron gas, whereas the decreasing deviation of the symmetric distribution from the thermal distribution describes thermalization (shaded areas). The complete relaxation of the electron gas from a hot distribution shortly after the excitation back to the equilibrium proceeds on times longer than 2.5 ps.

For a more quantitative discussion of the time scales of (i) orientational relaxation and (ii) thermalization and cooling, we connect the microscopic distributions in Eqs. (3) and (4) to observables.

(i) Orientational relaxation. To discuss the orientational relaxation time and to connect it to the Drude model, we study the macroscopic current density

$$\mathbf{j}(t) = -\frac{2e}{V}\sum_{\mathbf{k}} \mathbf{v}_{\mathbf{k}} f^{\rm non\text{-}sym}_{k_x,k_y,k_z}(t) \tag{5}$$

defined via the electron velocity $\mathbf{v}_{\mathbf{k}} = \frac{1}{\hbar}\frac{\partial \epsilon_k}{\partial \mathbf{k}}$. From symmetry considerations follows that the current density is carried exclusively by the nonsymmetric distribution $f^{\rm non\text{-}sym}_{k_x,k_y,k_z}$ [46]. This allows us to determine the effective orientational relaxation time $\tau_{\rm or}$ directly from the temporal decay of the current density, Eq. (5), shown in Fig. 4 (yellow line and inset). In the regime of linear excitations with $E_0/100$ (darkest line in the inset), the decay time corresponds to $\tau_{\rm or} = 19.7$ fs.

This orientational relaxation time $\tau_{\rm or}$ is obtained from the electron-phonon scattering in Eq. (1) as follows: Expanding the electron distribution $f_{\mathbf{k}}(t) = f_k^{\rm eq} + f^{\rm non\text{-}sym}_{\mathbf{k}}(t)$ up to first order perturbation in the linearly polarized light field, we derive the relaxation time approximation

$$\partial_t f^{\rm non\text{-}sym}_{\mathbf{k}}(t)|_{\rm OR} = -\gamma^{\rm or}_{\mathbf{k}}\left(f_{\mathbf{k}}(t) - f_k^{\rm eq}\right). \tag{6}$$

In this way, in the regime of linear optical excitation, the microscopic orientational relaxation rate

$$\gamma^{\rm or}_{\mathbf{k}} = \frac{4\pi}{\hbar k_B T_{\rm eq}} \sum_{\mathbf{q},\mathbf{G}} \left|g^{\mathbf{G}}_{\mathbf{q}}\right|^2 n(\hbar\omega_{\mathbf{q}}) n(-\hbar\omega_{\mathbf{q}}) \hbar\omega_{\mathbf{q}} \times \frac{|\mathbf{q}+\mathbf{G}|\cos(\sphericalangle \mathbf{k}, \mathbf{q}+\mathbf{G})}{k} \delta(\epsilon_{\mathbf{k}+\mathbf{q}+\mathbf{G}} - \epsilon_{\mathbf{k}} + \hbar\omega_{\mathbf{q}}) \tag{7}$$

represents a generalized, microscopic Bloch-Grüneisen formula for the metal resistivity. Note that the directional property of orientational relaxation is included in $\sphericalangle \mathbf{k}, \mathbf{q}+\mathbf{G}$ denoting the angle between $\mathbf{k}$ and $\mathbf{q}+\mathbf{G}$.

Clearly, these microscopic quantities, Eqs. (6) and (7), are connected with the macroscopic Drude model: The coarse-grained approach for the current density, Eq. (5), applied to Eq. (6) yields

$$\partial_t \mathbf{j}(t)|_{\rm OR} = \frac{2e}{V}\sum_{\mathbf{k}} \gamma^{\rm or}_{\mathbf{k}} \mathbf{v}_{\mathbf{k}} f^{\rm non\text{-}sym}_{\mathbf{k}}(t) \to -\left\langle \gamma^{\rm or}_{\mathbf{k}_F}\right\rangle_{\rm FS} \mathbf{j}(t).$$

Here, we introduce a macroscopic, momentum averaged orientational relaxation rate $\tau_{\rm or}^{-1}$ for the current decay by averaging $\gamma^{\rm or}_{\mathbf{k}}$ over the most relevant scattering processes close to the Fermi surface (FS) such that $\tau_{\rm or}^{-1} \langle \gamma^{\rm or}_{\mathbf{k}_F}\rangle_{\rm FS}$. A comparison with the classical Drude equation of motion [47,48]

$$\partial_t \mathbf{j}(t) = -\tau_D^{-1}\mathbf{j}(t) + \varepsilon_0 \omega_p^2 \mathbf{E}_0(t), \quad \text{with } \tau_D^{-1} \equiv \left\langle \gamma^{\rm or}_{\mathbf{k}_F}\right\rangle_{\rm FS}$$

reveals that the phenomenologically introduced Drude relaxation rate τ_D^{-1} corresponds to the macroscopical orientational relaxation rate $\tau_{\rm or}^{-1}$. Moreover, the identification of $\tau_{\rm or} = \tau_D$ allows a comparison with experimental studies of the optical dielectric function of gold. Here, Drude relaxation times between 9 fs and 26 fs for excitations below the optical band gap [49–53] are obtained. *Ab initio* studies based on a relaxation time approximation compute values between 24.0 fs and

26.3 fs [30,32]. Both are in agreement with our results in the linear regime.

Beyond linear excitation, our full numerical results in Fig. 4 predict a decrease of the orientational relaxation time for excitation with nonlinear field strength E_0 to $\tau_{\mathrm{or}} = 17.1$ fs (brightest line in the inset).

This implies a reduction of the orientational relaxation time for nonlinear excitations, when the acceleration energy ϵ_{ac} is at least in the same order as the thermal broadening $k_B T_{\mathrm{eq}}$ and the electron gas becomes strongly momentum polarized. However, a simplified relaxation time approximation as in Eq. (7) is not possible in the regime of nonlinear excitations as they lead to significant perturbations of the equilibrium distribution. The consequences of the nonlinearity in orientational relaxation on the optical properties of thin gold films are systematically discussed in Ref. [27].

(ii) Energy relaxation. In the regime of linear excitations, the energy transfer by the light field to the electron gas is negligible ($\epsilon_{\mathrm{ac}} \ll k_B T_{\mathrm{eq}}$) and a discussion of thermalization and cooling is unnecessary. In the nonlinear regime, energy relaxation occurs for nonthermal and thermal electrons via energetic redistribution and dissipation, respectively.

To access the dynamics of nonthermal electrons, we define the nonthermal energy density [10]

$$u_e^{\text{non-th}}(t) = \frac{1}{\pi^2} \int_0^\infty dk k^2 \epsilon_k \left(f_{|\mathbf{k}|}^{\mathrm{sym}}(t) - f_{|\mathbf{k}|}^{\mathrm{th}}(t) \right).$$

The thermal distribution is addressed by a Fermi-Dirac function

$$f_{|\mathbf{k}|}^{\mathrm{th}}(t) = \frac{1}{\exp \frac{\epsilon_k - \langle \mu(t) \rangle}{k_B \langle T_e(t) \rangle} + 1},$$

where the effective temperature $\langle T_e \rangle$ and the chemical potential $\langle \mu \rangle$ are defined by the slope of the function $\Phi_{|\mathbf{k}|}^{\mathrm{sym}}$ at the Fermi level (cf. Fig. 3). The relative fitting error of $\langle T_e \rangle$ depicted in Fig. 4 is less than 0.36%. The error is largest shortly after excitation, when orientational relaxation and thermalization are in progress, and drops to almost zero at longer times of several hundred fs.

As shown in Fig. 4, thermalization analyzed in terms of the nonthermal energy density, reveals a complex relaxation dynamics on a time up to $\tau_{\mathrm{th}}^{\mathrm{ep}} \approx 2.0$ ps. The observation of the backflow of nonthermal energy $|u^{\text{non-th}}|$ between 0.1 ps and 0.8 ps has already been reported for electron-phonon scattering [40,54,55] as well as electron-electron scattering [7]. Thermalization, described by electron-phonon interaction, is in agreement with observations in Refs. [10,11].

Simultaneous to thermalization, the electron gas dissipates thermal energy to the phonon bath in a cooling time $\tau_c = 0.8$ ps (red line in Fig. 4). Since heating and cooling of the electron gas are in a microscopic picture intrinsically nonlinear processes, the exact times depend on the strength of the light field and increase with increasing excitation strength. Similar cooling times in gold are provided by versatile experimental and theoretical approaches between 0.8 ps and 1.2 ps [8,56–61].

Finally, the electron gas reaches the thermodynamic equilibrium after about 2.5 ps, when the nonthermal distribution is decayed completely and the temperature $\langle T_e \rangle = T_e = T_{\mathrm{eq}}$ becomes a state function of the full electron gas [22,62].

Conclusion. We studied a momentum-resolved Boltzmann equation for bulk gold to fill the gap between ultrafast optical excitation providing a momentum-polarized electron gas to its energy-resolved thermalization and cooling. During orientational relaxation, the nonsymmetric electron distribution dominates for short times less than 100 fs directly after the excitation. For nonlinear excitations, energy relaxation proceeds via thermalization and cooling in about 2.5 ps. While in the linear regime the orientational relaxation rate is equivalent to the damping in the Drude model of approximately 20 fs, all three relaxation processes depend on the excitation strength in the nonlinear regime. In future work, the impact of electron-electron interaction, which is expected to be minor for orientational relaxation [63], has to be examined to achieve a complete picture of ultrafast electron relaxation in noble metals. In addition, as shown in Ref. [27], a self-consistent treatment of Maxwell's equations is necessary to describe the dephasing of optical and plasmonic excitations in spatially finite nanostructures. All in all, we believe that extending the momentum-resolved theory on more advanced systems could reveal new insights into the dephasing of plasmonic excitations [64,65].

Acknowledgments. We acknowledge fruitful discussions with Robert Salzwedel, Malte Selig, Lara Greten, Joris Sturm, Robert Lemke (TU Berlin), Francesca Calegari (DESY Hamburg), and Holger Lange (Uni Potsdam). A.K. acknowledges financial support from the Deutsche Forschungsgemeinschaft (DFG) through Project No. 556436549.

Data availability. The data that support the findings of this article are openly available [66].

[1] F. Krausz and M. I. Stockman, Attosecond metrology: From electron capture to future signal processing, Nat. Photon. **8**, 205 (2014).

[2] F. Calegari, G. Sansone, S. Stagira, C. Vozzi, and M. Nisoli, Advances in attosecond science, J. Phys. B: At. Mol. Opt. Phys. **49**, 062001 (2016).

[3] M. R. Bionta, F. Ritzkowsky, M. Turchetti, Y. Yang, D. Cattozzo Mor, W. P. Putnam, F. X. Kärtner, K. K. Berggren, and P. D. Keathley, On-chip sampling of optical fields with attosecond resolution, Nat. Photon. **15**, 456 (2021).

[4] M. R. Bionta, E. Haddad, A. Leblanc, V. Gruson, P. Lassonde, H. Ibrahim, J. Chaillou, N. Emond, M. R. Otto, A. Jimenez-Galan, R. E. F. Silva, M. Ivanov, B. J. Siwick, M. Chaker, and F. Legare, Tracking ultrafast solid-state dynamics using high harmonic spectroscopy, Phys. Rev. Res. **3**, 023250 (2021).

[5] D. A. Zimin, N. Karpowicz, M. Qasim, M. Weidman, F. Krausz, and V. S. Yakovlev, Dynamic optical response of solids following 1-fs-scale photoinjection, Nature (London) **618**, 276 (2023).

[6] K.-F. Wong, W. Li, Z. Wang, V. Wanie, E. Månsson, D. Hoeing, J. Blöchl, T. Nubbemeyer, A. Azzeer, A. Trabattoni, H. Lange, F. Calegari, and M. F. Kling, Far-Field petahertz sampling of plasmonic fields, Nano Lett. **24**, 5506 (2024).

[7] C. Seibel, M. Uehlein, T. Held, P. N. Terekhin, S. T. Weber, and B. Rethfeld, Time-Resolved spectral densities of nonthermal electrons in gold, J. Phys. Chem. C **127**, 23349 (2023).

[8] N. Del Fatti, C. Voisin, M. Achermann, S. Tzortzakis, D. Christofilos, and F. Vallée, Nonequilibrium electron dynamics in noble metals, Phys. Rev. B **61**, 16956 (2000).

[9] L. D. Pietanza, G. Colonna, S. Longo, and M. Capitelli, Non-equilibrium electron and phonon dynamics in metals under femtosecond laser pulses, Eur. Phys. J. D **45**, 369 (2007).

[10] B. Rethfeld, A. Kaiser, M. Vicanek, and G. Simon, Ultrafast dynamics of nonequilibrium electrons in metals under femtosecond laser irradiation, Phys. Rev. B **65**, 214303 (2002).

[11] B. Y. Mueller and B. Rethfeld, Relaxation dynamics in laser-excited metals under nonequilibrium conditions, Phys. Rev. B **87**, 035139 (2013).

[12] S. Ono and T. Suemoto, Ultrafast photoluminescence in metals: Theory and its application to silver, Phys. Rev. B **102**, 024308 (2020).

[13] D. M. Riffe and R. B. Wilson, Excitation and relaxation of non-thermal electron energy distributions in metals with application to gold, Phys. Rev. B **107**, 214309 (2023).

[14] G. V. Hartland, Coherent vibrational motion in metal particles: Determination of the vibrational amplitude and excitation mechanism, J. Chem. Phys. **116**, 8048 (2002).

[15] R. Salzwedel, A. Knorr, D. Hoeing, H. Lange, and M. Selig, Theory of radial oscillations in metal nanoparticles driven by optically induced electron density gradients, J. Chem. Phys. **158**, 064107 (2023).

[16] C.-K. Sun, F. Vallée, L. H. Acioli, E. P. Ippen, and J. G. Fujimoto, Femtosecond-tunable measurement of electron thermalization in gold, Phys. Rev. B **50**, 15337 (1994).

[17] G. Della Valle, M. Conforti, S. Longhi, G. Cerullo, and D. Brida, Real-time optical mapping of the dynamics of nonthermal electrons in thin gold films, Phys. Rev. B **86**, 155139 (2012).

[18] Y. Sivan and S.-W. Chu, Nonlinear plasmonics at high temperatures, Nanophotonics **6**, 317 (2017).

[19] P. D. Ndione, S. T. Weber, D. O. Gericke, and B. Rethfeld, Nonequilibrium band occupation and optical response of gold after ultrafast XUV excitation, Sci. Rep. **12**, 4693 (2022).

[20] A. Schirato, M. Maiuri, G. Cerullo, and G. D. Valle, Ultrafast hot electron dynamics in plasmonic nanostructures: Experiments, modeling, design, Nanophotonics **12**, 1 (2023).

[21] P. B. Allen, Theory of thermal relaxation of electrons in metals, Phys. Rev. Lett. **59**, 1460 (1987).

[22] Y. Dubi and Y. Sivan, "Hot" electrons in metallic nanostructures—non-thermal carriers or heating? Light Sci. Appl. **8**, 89 (2019).

[23] Y. Sivan and Y. Dubi, Theory of "hot" photoluminescence from drude metals, ACS Nano **15**, 8724 (2021).

[24] S. Sarkar, I. W. Un, and Y. Sivan, Electronic and thermal response of low-electron-density drude materials to ultrafast optical illumination, Phys. Rev. Appl. **19**, 014005 (2023).

[25] M. Maiuri, M. Garavelli, and G. Cerullo, Ultrafast spectroscopy: State of the art and open challenges, J. Am. Chem. Soc. **142**, 3 (2020).

[26] F. Boschini, M. Zonno, and A. Damascelli, Time-resolved ARPES studies of quantum materials, Rev. Mod. Phys. **96**, 015003 (2024).

[27] J. Grumm, M. Selig, H. Lange, and A. Knorr, companion paper, Theory of nonlinear electron relaxation in thin gold films and their signatures in optical observables, Phys. Rev. B **112**, 245402 (2025).

[28] J. Ziman, *Electrons and Phonons* (Clarendon Press, Oxford, 1960).

[29] W. E. Lawrence and J. W. Wilkins, Umklapp electron-phonon scattering in the low-temperature resistivity of polyvalent metals, Phys. Rev. B **6**, 4466 (1972).

[30] A. M. Brown, R. Sundararaman, P. Narang, W. A. Goddard, and H. A. Atwater, Nonradiative plasmon decay and hot carrier dynamics: Effects of phonons, surfaces, and geometry, ACS Nano **10**, 957 (2016).

[31] A. M. Brown, R. Sundararaman, P. Narang, W. A. Goddard, and H. A. Atwater, *Ab initio* Phonon coupling and optical response of hot electrons in plasmonic metals, Phys. Rev. B **94**, 075120 (2016).

[32] J. I. Mustafa, M. Bernardi, J. B. Neaton, and S. G. Louie, *Ab initio* Electronic relaxation times and transport in noble metals, Phys. Rev. B **94**, 155105 (2016).

[33] R. Sundararaman, P. Narang, A. S. Jermyn, W. A. Goddard III, and H. A. Atwater, Theoretical predictions for hot-carrier generation from surface plasmon decay, Nat. Commun. **5**, 5788 (2014).

[34] G. D. Mahan, *Solid State Physics*, 3rd ed. (Springer Science + Business Media, New York, 2000).

[35] N. W. Ashcroft and N. D. Mermin, *Solid State Physics* (Hartcourt College Publishers, London, 1976).

[36] T. Meier, G. von Plessen, P. Thomas, and S. W. Koch, Coherent electric-field effects in semiconductors, Phys. Rev. Lett. **73**, 902 (1994).

[37] R. H. M. Groeneveld, R. Sprik, and A. Lagendijk, Femtosecond spectroscopy of electron-electron and electron-phonon energy relaxation in Ag and Au, Phys. Rev. B **51**, 11433 (1995).

[38] S. D. Brorson, A. Kazeroonian, J. S. Moodera, D. W. Face, T. K. Cheng, E. P. Ippen, M. S. Dresselhaus, and G. Dresselhaus, Femtosecond room-temperature measurement of the electron-phonon coupling constant γ in metallic superconductors, Phys. Rev. Lett. **64**, 2172 (1990).

[39] V. V. Kabanov and A. S. Alexandrov, Electron relaxation in metals: Theory and exact analytical solutions, Phys. Rev. B **78**, 174514 (2008).

[40] S. Ono, Thermalization in simple metals: Role of electron-phonon and phonon-phonon scattering, Phys. Rev. B **97**, 054310 (2018).

[41] E. N. Adams, The crystal momentum as a quantum mechanical operator, J. Chem. Phys. **21**, 2013 (1953).

[42] W. S. Fann, R. Storz, H. W. K. Tom, and J. Bokor, Electron thermalization in gold, Phys. Rev. B **46**, 13592 (1992).

[43] E. Malic, T. Winzer, and A. Knorr, Efficient orientational carrier relaxation in optically excited graphene, Appl. Phys. Lett. **101**, 213110 (2012).

[44] M. Mittendorff, T. Winzer, E. Malic, A. Knorr, C. Berger, W. A. De Heer, H. Schneider, M. Helm, and S. Winnerl, Anisotropy of excitation and relaxation of photogenerated charge carriers in graphene, Nano Lett. **14**, 1504 (2014).

[45] R. Binder, H. S. Köhler, M. Bonitz, and N. Kwong, Green's function description of momentum-orientation relaxation of photoexcited electron plasmas in semiconductors, Phys. Rev. B **55**, 5110 (1997).

[46] O. Hess and T. Kuhn, Maxwell-Bloch equations for spatially inhomogeneous semiconductor lasers. I. Theoretical formulation, Phys. Rev. A **54**, 3347 (1996).

[47] P. Drude, Zur elektronentheorie der metalle, Ann. Phys. (NY) **306**, 566 (1900).

[48] S. A. Maier, *Plasmonics: Fundamentals and Applications* (Springer, New York, 2007), Vol. 1.

[49] P. B. Johnson and R. W. Christy, Optical constants of the noble metals, Phys. Rev. B **6**, 4370 (1972).

[50] M. A. Ordal, R. J. Bell, R. W. Alexander, L. L. Long, and M. R. Querry, Optical properties of Au, Ni, and Pb at submillimeter wavelengths, Appl. Opt. **26**, 744 (1987).

[51] S. Babar and J. H. Weaver, Optical constants of Cu, Ag, and Au revisited, Appl. Opt. **54**, 477 (2015).

[52] M. Magnozzi, M. Ferrera, L. Mattera, M. Canepa, and F. Bisio, Plasmonics of Au nanoparticles in a hot thermodynamic bath, Nanoscale **11**, 1140 (2019).

[53] R. L. Olmon, B. Slovick, T. W. Johnson, D. Shelton, S.-H. Oh, G. D. Boreman, and M. B. Raschke, Optical dielectric function of gold, Phys. Rev. B **86**, 235147 (2012).

[54] K. Inayoshi, A. Koga, and Y. Murakami, Energy flow during relaxation in an electron–phonon system with multiple modes: A nonequilibrium Green's function study, J. Phys. Soc. Jpn. **92**, 124001 (2023).

[55] U. Ritzmann, P. M. Oppeneer, and P. Maldonado, Theory of out-of-equilibrium electron and phonon dynamics in metals after femtosecond laser excitation, Phys. Rev. B **102**, 214305 (2020).

[56] W. S. Fann, R. Storz, H. W. K. Tom, and J. Bokor, Direct measurement of nonequilibrium electron-energy distributions in subpicosecond laser-heated gold films, Phys. Rev. Lett. **68**, 2834 (1992).

[57] C.-K. Sun, F. Vallée, L. Acioli, E. P. Ippen, and J. G. Fujimoto, Femtosecond investigation of electron thermalization in gold, Phys. Rev. B **48**, 12365 (1993).

[58] A. Giri, J. T. Gaskins, B. M. Foley, R. Cheaito, and P. E. Hopkins, Experimental evidence of excited electron number density and temperature effects on electron-phonon coupling in gold films, J. Appl. Phys. **117**, 044305 (2015).

[59] A. M. Brown, R. Sundararaman, P. Narang, A. M. Schwartzberg, W. A. Goddard, and H. A. Atwater, Experimental and *ab initio* ultrafast carrier dynamics in plasmonic nanoparticles, Phys. Rev. Lett. **118**, 087401 (2017).

[60] Z. Zhang, C. Zhang, H. Zheng, and H. Xu, Plasmon-driven catalysis on molecules and nanomaterials, Acc. Chem. Res. **52**, 2506 (2019).

[61] T. Suemoto, K. Yamanaka, N. Sugimoto, Y. Kobayashi, T. Otsu, S. Tani, and T. Koyama, Relaxation dynamics of hot electrons in the transition metals Au, Ag, Cu, Pt, Pd, and Ni studied by ultrafast luminescence spectroscopy, J. Appl. Phys. **130**, 025101 (2021).

[62] A. Puglisi, A. Sarracino, and A. Vulpiani, Temperature in and out of equilibrium: A review of concepts, tools and attempts, Phys. Rep. **709–710**, 1 (2017).

[63] W. E. Lawrence and J. W. Wilkins, Electron-Electron scattering in the transport coefficients of simple metals, Phys. Rev. B **7**, 2317 (1973).

[64] R. Zhang, L. Bursi, J. D. Cox, Y. Cui, C. M. Krauter, A. Alabastri, A. Manjavacas, A. Calzolari, S. Corni, E. Molinari, E. A. Carter, F. J. G. De Abajo, H. Zhang, and P. Nordlander, How to identify plasmons from the optical response of nanostructures, ACS Nano **11**, 7321 (2017).

[65] M. Ferrera, G. Della Valle, M. Sygletou, M. Magnozzi, D. Catone, P. O'Keeffe, A. Paladini, F. Toschi, L. Mattera, M. Canepa, and F. Bisio, Thermometric calibration of the ultrafast relaxation dynamics in plasmonic au nanoparticles, ACS Photon. **7**, 959 (2020).

[66] J. Grumm, Dataset for femtosecond dynamics of electrons in noble metals: Orientational relaxation in momentum space and the drude relaxation rate, Zenodo (2025), available at: https://zenodo.org/records/16994957.